AKAP18:PKA-RIIα structure reveals crucial anchor points for recognition of regulatory subunits of PKA

Goetz, F., Roske, Y., Schulz, M.S., Autenrieth, K., Bertinetti, D., Faelber, K., Zuehlke, K., Kreuchwig, A., Kennedy, E., Krause, G., Daumke, O., Herberg, F.W., Heinemann, U., Klussmann, E.

Biochemical Journal
2016 JUL 01 ; 473(13): 1881-1894
2016 JUN 28 (first published online: final publication)
doi: 10.1042/BCJ20160242

Publisher: Portland Press on behalf of the Biochemical Society

PORTLAND PRESS

BIOCHEMICAL JOURNAL
ACCEPTED MANUSCRIPT

AKAP18:PKA-RIIα structure reveals crucial anchor points for recognition of regulatory subunits of PKA

Frank Götz, Yvette Roske , Maike Svenja Schulz, Karolin Autenrieth, Daniela Bertinetti, Katja Faelber, Kerstin Zühlke, Annika Kreuchwig , Eileen Kennedy , Gerd Krause , Oliver Daumke, Friedrich W. Herberg, Udo Heinemann and Enno Klussmann

A-kinase anchoring proteins (AKAPs) interact with the dimerization/docking (D/D) domains of regulatory subunits of the ubiquitous protein kinase A (PKA). AKAPs tether PKA to defined cellular compartments establishing distinct pools to increase the specificity of PKA signalling. Here, we elucidated the structure of an extended PKA-binding domain of AKAP18β bound to the D/D domain of the regulatory RIIα subunits of PKA. We identified three hydrophilic anchor points in AKAP18β outside the core PKA-binding domain, which mediate contacts with the D/D domain. Such anchor points are conserved within AKAPs that bind regulatory RII subunits of PKA. We derived a different set of anchor points in AKAPs binding regulatory RI subunits of PKA. In vitro and cell-based experiments confirm the relevance of these sites for the interaction of RII subunits with AKAP18 and of RI subunits with the RI-specific smAKAP. Thus we report a novel mechanism governing interactions of AKAPs with PKA. The sequence specificity of each AKAP around the anchor points and the requirement of these points for the tight binding of PKA allow the development of selective inhibitors to unequivocally ascribe cellular functions to the AKAP18-PKA and other AKAP-PKA interactions.

Cite as Biochemical Journal (2016) DOI: 10.1042/BCJ20160242

AKAP18:PKA-RIIα structure reveals crucial anchor points for recognition of regulatory subunits of PKA

Frank Götz*¶[1], Yvette Roske*[1], Maike Svenja Schulz*, Karolin Autenrieth‡, Daniela Bertinetti‡, Katja Faelber*, Kerstin Zühlke*, Annika Kreuchwig¶, Eileen Kennedy#, Gerd Krause¶, Oliver Daumke*, Friedrich W. Herberg‡, Udo Heinemann* and Enno Klussmann*§[2]

[1]contributed equally

Affiliations

*Max Delbrück Center for Molecular Medicine Berlin in the Helmholtz Association (MDC), Robert-Rössle-Straße 10, 13125 Berlin, Germany,
¶Leibniz Institute for Molecular Pharmacology (FMP), Robert-Rössle-Straße 10, 13125 Berlin, Germany,
‡University of Kassel, Heinrich-Plett-Straße 40, Kassel, Germany
#University of Georgia, Athens, USA
§DZHK, German Centre for Cardiovascular Research, Oudenarder Straße 16,13347 Berlin, Germany

Short title: Anchor points for AKAP-PKA interactions

Keywords: A-kinase anchoring protein; protein kinase A; D/D domain; PKA-binding domain; protein-protein interaction; compartmentalized cAMP signalling

[2]**Address for correspondence**
Enno Klussmann
Max Delbrück Center for Molecular Medicine Berlin
in the Helmholtz Association (MDC)
Robert-Rössle-Str. 10
13125 Berlin
Germany
Tel. +49-30-9406 2596
FAX +49-30-9406 2593
E-mail: enno.klussmann@mdc-berlin.de

SUMMARY

A-kinase anchoring proteins (AKAPs) interact with the dimerization/docking (D/D) domains of regulatory subunits of the ubiquitous protein kinase A (PKA). AKAPs tether PKA to defined cellular compartments establishing distinct pools to increase the specificity of PKA signalling. Here, we elucidated the structure of an extended PKA-binding domain of AKAP18β bound to the D/D domain of the regulatory RIIα subunits of PKA. We identified three hydrophilic anchor points in AKAP18β outside the core PKA-binding domain, which mediate contacts with the D/D domain. Such anchor points are conserved within AKAPs that bind regulatory RII subunits of PKA. We derived a different set of anchor points in AKAPs binding regulatory RI subunits of PKA. *In vitro* and cell-based experiments confirm the relevance of these sites for the interaction of RII subunits with AKAP18 and of RI subunits with the RI-specific smAKAP. Thus we report a novel mechanism governing interactions of AKAPs with PKA. The sequence specificity of each AKAP around the anchor points and the requirement of these points for the tight binding of PKA allow the development of selective inhibitors to unequivocally ascribe cellular functions to the AKAP18-PKA and other AKAP-PKA interactions.

INTRODUCTION

A-kinase anchoring proteins (AKAPs) are a diverse family of around 50 scaffolding proteins with molecular weights ranging from 18 to more than 500 kDa. They share the capacity to directly interact with protein kinase A (PKA) and thereby to tether the kinase to defined cellular sites. This controls PKA signalling spatially and temporally and confers specificity to the action of this ubiquitous kinase. However, AKAPs' functions are not restricted to controlling PKA activity. AKAPs integrate cellular signalling processes by forming multi-protein complexes through direct protein-protein interactions with PKA substrates and other signalling proteins, such as further kinases, phosphodiesterases (PDEs) or phosphatases (PPs); their unique anchoring domains tether AKAP-based protein complexes to defined cellular compartments [1-6].

PKA consists of a dimer of regulatory RI (RIα or RIβ) or RII (RIIα or RIIβ) and two catalytic subunits (Cα, β or γ), each bound to one R subunit [7]. The regulatory subunits of PKA dimerize through interaction of their N terminal dimerization/docking (D/D) domains (amino acids 1-44). The dimerized D/D domains form a hydrophobic cavity into which the A-kinase-binding domains (AKB) of AKAPs dock. AKAPs can only interact with dimers of regulatory subunits. A few AKAPs can bind both RI and RII subunits (dual specific AKAPs) [8, 9], most AKAPs preferentially bind RII [10, 11], and some preferentially or specifically bind RI, such as SKIP [12, 13] and smAKAP [14].

NMR analysis has revealed the 3D structure of the D/D domain of RIIα in complex with the AKBs of AKAP-Lbc (peptide Ht31(493-515); 23 amino acids) [15] and of AKAP79 (peptide AKAP79(392-408); 16 amino acids) [15, 16]. X-ray crystallography resolved 3D structures of the AKBs of D-AKAP2 (amino acid residues 631-651; 20 amino acids) [17] and of the *in silico*-designed AKAP-*IS* (amino acid residues 4-20; 16 amino acid residues) [18] with the D/D domain of RIIα. All structures show that AKBs are amphipathic helices. The hydrophobic face of the helix docks into the hydrophobic cavity formed by the D/D domains, which have an X-type helix bundle conformation. Thus hydrophobic interactions are considered the backbone of the binding. Comparison with additional AKAPs indicates that the amphipathic helix is a conserved motif within the AKAP family mediating the interaction with D/D domains. The conserved positioning of hydrophobic amino acid residues allowed defining an AKAP signature motif: *H*xx*HH*xx*HH*xx*HH*xx*HH*, where *H* denotes hydrophobic amino acid residues in conserved positions of AKBs, x stands for any amino acid residue [19]. Database screening for this motif, combined with the pI range of known AKBs (3.43 to 6.23) or with the available structural information, has identified novel AKAPs [19, 20]. There are hints that allosteric sites such as the RI Specifier Region (RISR) in D-AKAPs [21] and a region C-terminally from the D/D domain of RIIα [22] are involved in AKAP-PKA interactions but there is no support from structural analyses.

Interactions between AKAPs and PKA are involved in an array of cellular processes including vasopressin-mediated water reabsorption in renal principal cells [23, 24], cardiac myocyte contractility [25] or lipolysis in adipocytes [26, 27]. AKAP18 (AKAP7) comprises a family of four isoforms, AKAP18α, β, γ and δ (Supplementary Figure 1), of which the α, β and γ isoforms are expressed in humans while the δ isoform is found in rat [10, 28-31]. AKAP18α (also termed AKAP15 or AKAP7α) is one of three AKAPs interacting with L-type Ca^{2+} channels in cardiac myocytes. AKAP18α is believed to facilitate the phosphorylation of the channel by PKA and thereby to increase Ca^{2+} entry [31]. Compared to AKAP18α, AKAP18β carries an insert of 23 amino acid residues in its N terminus, which leads to apical plasma membrane localization of the AKAP-PKA complex [30]. AKAP18γ forms a complex with PKA, sarcoplasmic reticulum Ca^{2+} ATPase 2 (SERCA2) and PDE3A1 in human myocardium. These interactions participate in the control of Ca^{2+} reuptake into the sarcoplasmic reticulum during diastole [32]. The interaction of AKAP18δ with PKA and phospholamban controls Ca^{2+} reuptake into the sarcoplasmic reticulum of rat cardiac myocytes [33], and apparently plays a role in the control of vasopressin-mediated water reabsorption in renal principal cells [10].

The various biological functions of AKAP-PKA interactions have mainly been revealed by inhibition with synthetic membrane-permeant peptides. Peptides derived from AKBs of AKAPs such as AKAP-Lbc (peptide Ht31) or AKAP18δ (peptide AKAP18δL314E) bind regulatory subunits of PKA with nanomolar affinity and thereby globally uncouple PKA from AKAPs [4, 34, 35]. More recent studies led to peptides that preferentially disrupt AKAP-RI or AKAP-RII interactions [36-41]. However, no agent for selective disruption of any defined AKAP-PKA interaction is available to date; the closest are peptides derived from regulatory subunits of PKA that preferentially interfere with AKAP18-PKA or AKAP79-PKA interactions [42]. The lack of specific inhibitors of defined AKAP-PKA interactions impairs the unequivocal ascription of particular functions. One prerequisite for understanding the molecular mechanisms underlying specific interactions and the design of selective inhibitors is the elucidation of 3D structures of individual AKAP-PKA complexes.

Here, we report the 3D structure of a complex of an extended AKB of AKAP18β with the D/D domain of RIIα, which reveals a novel binding frame for RIIα, mediated by conserved anchor points in the AKAP sequence. Such anchor points are present in other AKAPs. These sites provide unique opportunities for specific pharmacological interference with a defined AKAP-PKA interaction.

EXPERIMENTAL

Cloning and generation of recombinant AKAP18β and D/D domain of RIIα

An AKAP18β cDNA fragment encoding amino acid residues 43-83 (NGGEP DDAEL VRLSK RLVEN AVLKA VQQY LEETQ NKNKP GE) was cloned by ligation-independent cloning (LIC) into vector pET30 Ek/LIC (Merck Millipore, Darmstadt, Germany). PCR was used for introduction of an additional PreScission recognition site for His-tag removal. The AKAP18β(43-83) encoding cDNA fragment was amplified from a pCMV6-XL5 clone (Origene, NM_138633), purified, and 0.2 pmol were treated with T4 DNA polymerase, annealed with the vector pET30 Ek/LIC, which was transformed into *E. coli* strain NovaBlue GigaSingles competent cells (Novagen). The untagged RIIα-D/D domain (amino acids 1-44) was cloned into pET46 by removing the N-terminal His-tag from His-D/D RIIα in pET46 Ek/LIC [43] by PCR with the primer pair forward-DD: 5'-GGTCA GCCAT GGCAA GCCAC ATCCA GAT-3' and reverse-DD: 5'-CGTCT TCTCG AGTTA GCGGG CCTCG CG-3' and restriction with NcoI/XhoI.

For crystallization, the two proteins were co-expressed in *E. coli* strain Rosetta 2 DE3 in the presence of the antibiotics kanamycin, ampicillin, and chloramphenicol. Pre-cultures from cryo stocks were grown in 50 ml LB medium at 37 °C overnight, centrifuged and resuspended to inoculate up to four 500 ml Overnight Express™ Instant TB Medium (autoinduction medium; Novagen). Cultures were grown for at least 24 h at 37 °C under constant agitation (110 rpm) in 2 l Erlenmeyer flasks. Cells were harvested by centrifugation, washed with PBS and stored at -80 °C.

Lysates were prepared in 40 mM phosphate buffer, pH 7.5, 300 mM NaCl, 5 mM imidazole, 2 mM $MgCl_2$, 5 mM β-mercaptoethanol, 0.5 mM PMSF, Roche Protease Inhibitor tablet, benzonase (5 µl/100 ml) using a fluidizer. Cell debris was removed by centrifugation at 21,000 rpm at 4 °C for 30 min. The supernatant was cleared by filtration through a 0.45 µm filter and applied to a TALON cobalt affinity column (Clontech) in an ÄKTA system pre-equilibrated with 40 mM phosphate buffer, pH 7.5, 300 mM NaCl, 5 mM imidazole. The TALON column was washed with equilibration buffer with 10 mM imidazole and eluted with 40 mM phosphate buffer, pH 7.5, 300 mM NaCl and an imidazole gradient up to 300 mM. His-AKAP18β(43-83):RIIα-D/D complex containing fractions were pooled. After dialysis against 20 mM phosphate, pH 7.5, 150 mM NaCl, 2 mM $MgCl_2$, the His-tag of AKAP18β(43-83) was removed overnight with His-PreScission protease. His-tag and His-PreScission were separated from tag-free AKAP18β(43-83):RIIα-D/D complex by TALON cobalt affinity column chromatography under identical buffer conditions. The final polishing step was a gel filtration with a HiLoad 16/600 Superdex 75 (GE Healthcare) in 20 mM HEPES, pH 7.5, 150 mM NaCl, 0.2 mM $MgCl_2$. The purest fractions were pooled and stored at -80 °C.

For interaction studies with ITC (or Biacore), a double mutant of AKAP18β(43-83), AKAP18β(43-83)D49A/E74A, and a triple mutant, AKAP18β(43-83)D49A/Q70A/E74A in pET30 Ek/LIC-AKAP18β(43-83) were generated. The corresponding point mutations were introduced into pET30 Ek/LIC AKAP18β(43-83) in three consecutive rounds of PCRs by using Pfu Ultra II polymerase (primer pair forward-AK18β-D49A: 5'-GGAGG GGAGC CCGAT GCCGC TGAAC TAGTA AGG-3' with reverse-AK18β-D49A: 5'-CCTTA CTAGT TCAGC GGCAT CGGGC TCCCC TCC-3', and primer pair forward-AK18β-E74A: 5'-GTCCA GCAGT ATCTG GAGGC AACA CAGAA TAAAA AC-3' with reverse-AK18β-E74A: 5'-GTTTT TATTC TGTGT TGCCT CCAGA TACTG CTGGA C-3' to generate the double mutant AKAP18β(43-83)D49A/E74A and primer pair forward-AK18β-Q70A: 5'- GCTCA AGGCT GTCCA GGCGT ATCTG GAGGC AACA-3' with reverse-AK18β-Q70A: 5'- TGTTG CCTCC AGATA CGCCT GGACA GCCTT GAGC-3' to obtain the triple mutant AKAP18β(43-83)D49A/Q70A/E74A). After DpnI digestion, the reactions were transformed in Strata Clone Solo Pack competent cells (Agilent). Mutations were verified by sequencing. AKAP18β(43-83), AKAP18β(43-

83)D49A/E74A and AKAP18β(43-83)D49A/Q70A/E74A were expressed in *E. coli* (strain Rosetta 2 DE3) in the presence of the antibiotics kanamycin and chloramphenicol. Purification of the proteins was carried out as described above for the AKAP18β(43-83):RIIα-D/D domain complex. D/D domain of RIIα or full-length RIIα were obtained as previously described [43].

Crystallization and data collection

The purified complex AKAP18β(43-83):RIIα-D/D (1-44) was concentrated to 49 mg/ml and was mixed with an equal volume (200 nl) of reservoir solution containing 21% PEG3350, 10 mM $CdCl_2$ hydrate, 0.1 M NaOAc, pH 4.5. The crystallization experiments were performed using the sitting-drop vapour-diffusion method at 20 °C with a Gryphon pipetting robot (Matrix Technologies Corporation) and a Rock Imager 1000 storage system (Formulatrix).
Crystals of the complex appeared after 2-3 weeks and were flash-frozen in liquid nitrogen in a cryo-solution containing additionally 20 % glycerol relative to the reservoir solution. Diffraction data were collected on BL14.1 operated by the Helmholtz-Zentrum Berlin (HZB) at the BESSY II electron storage ring (Berlin-Adlershof, Germany). The data were processed and scaled using the XDSAPP suite [44].

Structure determination

Phases for the AKAP18β:RIIα-D/D complex were obtained by molecular replacement with PHASER [45] using the RIIα-D/D domain of the AKAP-*IS*:RIIα-D/D domain complex (PDB: 2IZX) as search model [18]. The AKAP18β:RIIα-D/D complex structure was manually built using COOT [46] and iteratively refined using REFMAC. Two prominent electron density maxima at the centre of the AKAP18β:RIIα-D/D pseudo-trimer (see Results) were assigned as Cd^{2+} positions based on the presence of $CdCl_2$ in the crystallization buffer. The presence of Cd^{2+} was inferred from the short distances of the Cd-O bonds (typically 2-2.5 Å) and the coordination geometry [47]. Data collection and refinement statistics are reported in Table 1. Analysis with MolProbity (http://molprobity.biochem.duke.edu/) shows that 98.5 % of the modelled residues are in favoured regions of the Ramachandran map with no outliers. Figures were prepared with PyMOL Molecular Graphics System (Version 1.3, Schrödinger, LLC). Domain superimpositions were also performed with PyMOL, which aligns the sequences and computes a structural alignment with several cycles of refinement in order to reject structural outliers found during the fit. The angle calculation of the AKAP helices bound to the D/D dimers were performed with the Python module “anglebetweenhelices” implemented in PyMOL.

Static light scattering (SLS)

SLS experiments were carried out employing a Superdex 75 10/300 SEC analytical column attached to an ÄKTA FPLC system (both GE Healthcare) coupled to VE3580 RI and 270 Dual detectors (Viscotek). Evaluation of the data was performed using the OmniSec software (Viscotek) and the RI signal. The protein concentration of the complex AKAP18β(43-83):RIIα-D/D(1-44) was adjusted to 200 µM in 20 mM HEPES, 150 mM NaCl, pH 7.5, complemented with 2 mM $CdCl_2$ or 2 mM EDTA. All samples were injected in 200 µl aliquots. The Superdex 75 10/300 column was equilibrated with the same buffer, and run at a flow rate of 0.5 ml/min.

Analytical ultracentrifugation

Sedimentation velocity experiments of the complex AKAP18β(43-83):RIIα-D/D(1-44) were carried out at 20 °C with an Optima XL-i analytical ultracentrifuge (Beckman) at 35,000 rpm with a 60-Ti rotor (Beckman Instruments). The analysed samples were prepared in 20 mM HEPES, 150 mM NaCl, pH 7.5 with either 2 mM $CdCl_2$ or 2 mM EDTA at a protein concentration of 0.6 mg/ml. Two-channel Epon centrepieces with an optical path of 12 mm were used,

and all experiments were performed using sapphire windows. Scans were recorded at 280 nm with radial spacing of 0.005 cm. The program Sednterp was used to estimate the partial specific volume from amino acid composition as well as the density ρ and viscosity η. Data were then analysed with the program SEDFIT [48] using a continuous *c*(s) distribution model. Theoretical sedimentation coefficients for monomeric and higher oligomeric protein species were calculated using the following equation

$$s = \frac{M_W(1-\rho)}{N_A(f/f_0)6\pi\eta\sqrt[3]{3M/\pi N_A}}$$

with N_A Avogadro's number and M_W and f/f_0 the protein's molecular weight and frictional ratio, respectively. Assuming a frictional ratio of 1.25, theoretical sedimentation coefficients of 1.7 and 2.2 were calculated for a monomeric or dimeric complex, respectively (one copy of AKAP18β(43-83) and two copies of RIIα D/D(1-44). The monomeric complex has a molecular weight of 15.0 kDa.

In silico binding energy estimation

The free energies of binding ΔG_{bind} (kJ/mol) were estimated using the equation:

$$\Delta G_{bind} = G_{complex} - (G_{protein} + G_{ligand})$$

where $G_{complex}$ is the optimized free energy for the complex, $G_{protein}$ and G_{ligand} are the optimized free energy for the free D/D domain and free peptide, respectively. Each energy term was calculated by a combination of molecular mechanics energy, implicit solvation energy and surface area energy.

Isothermal Titration Calorimetry (ITC)

ITC experiments were performed in 20 mM HEPES, pH 7.5, 150 mM NaCl using a VP-ITC titration microcalorimeter (GE Healthcare, Freiburg, Germany). The D/D domain of RIIα (20 μM) was loaded into the calorimeter cell. The titration syringe was filled either with AKAP18β(43-83), AKAP18β(43-83)D49A/E74A or AKAP18β(43-83)D49A/Q70A/E74A at 100 μM. Titrations were carried out using 25-30 injections of 10-12 μl each injected at 5–20 min intervals at a constant temperature of 25 °C. Raw data in the form of the incremental heat per mole of added protein were fitted with the ORIGIN7 software by non-linear least squares using a one-site binding model for the D/D domain of RIIα:AKAP18β(43-83) titration. The protein concentration was adjusted by this fit. In the case of the mutants AKAP18β(43-83)D49A/E74A and AKAP18β(43-83)D49A/Q70A/E74A fitting of the data to a one-site binding model was not possible.

Surface Plasmon Resonance Measurements

Interaction studies were performed using a Biacore T200 instrument (GE Healthcare, Freiburg, Germany). RIIα subunits were captured as previously described [49]. Measurements were performed in running buffer containing 20 mM MOPS, 150 mM NaCl, 3 mM EDTA, 0.05 % (v/v) surfactant P20, pH 7. In brief, 8-AHA-cAMP (BIOLOG Life Science Institute, Bremen, Germany) was covalently coupled to CM5 sensor chips (GE Healthcare, Freiburg, Germany) using standard NHS/EDC chemistry [50]. Each flow cell was activated, coupled and deactivated individually with a flow rate of 5 μl/min at 25 °C. Purified human PKA RIIα was injected in running buffer containing 2 mg/mL bovine serum albumin for reversibly capture on the 8-AHA-cAMP surface (surface density: 290 resonance units). An 8-AHA-cAMP surface without captured R subunit served as reference in order to test for unspecific binding. After each cycle, regeneration of the surface was performed by two short injections (15 s each) of 0.1 % (w/v) SDS, followed by a single injection of 3 M guanidinium hydrochloride (30 s) and an in-

jection of running buffer with 1 M NaCl (30 s). Kinetic analyses were performed by injection of increasing concentrations (0.2 nM – 146 nM) of the AKAP18β variants at a flow rate of 100 µl/min at 37 °C. Association signals were recorded for 60 s and the dissociation of the highest AKAP18β concentration (146 nM) was monitored for 2 h. After subtracting the reference cell signal, the resulting binding signals were evaluated with BIAevaluation software version 4.1.1. The dissociation phase was fitted separately using the same software.

Generation of Flag-AKAP18γ and Flag-smAKAP

The plasmids were generated by standard PCR using Pfu Ultra II polymerase. Full-length human AKAP18γ(D293A/Q314A/E318A) was generated by sequential mutagenesis of plasmid AKAP18γ (wild type AKAP18γ purchased as GeneArt Strings^{TM} DNA fragment, Life technologies and inserted into pCMV6-Entry, Origene, PS100001). The primer pairs for PCR were: forward-AK18γ-E318A: 5'-GTCCA GCAGT ATCTG GAGGC AACAC AGAAT AAAAAC-3' with reverse-AK18γ-E318A: 5'- GTTTT TATTC TGTGT TGCCT CCAGA TACTG CTGGAC-3', primer pair forward-AK18γ-Q314A: 5'-GCTCA AGGCT GTCCA GGCGT ATCTG GAGGC AACA-3' with reverse-AK18γ-Q314A: 5'-TGTTG CCTCC AGATA CGCCT GGACA GCCTT GAGC-3' and forward-AK18γ-D293A: 5'-GAGCC CGATG CCGCT GAACT AGTAA GGC-3' with reverse-AK18γD293A: 5'-GCCTT ACTAG TTCAG CGGCA TCGGG CTC-3'. After DpnI digestion Strata Clone Solo Pack competent cells (Agilent) were transformed with the DNAs. Mutations were confirmed by sequencing.
For the generation of wild type smAKAP and smAKAP(D72A/Q76A) synthetic DNA sequences (Eurofins genomics; sequences are shown in the supplementary information) were inserted into plasmid pCMV6-Entry (Origene, PS100001).

Cell culture, AKAP expression, immunoprecipitation and Western blotting

HEK293 cells were grown in DMEM (GlutaMAX, 10 % FCS, Thermo Fisher Scientific, Waltham, USA) and transfected with the abovementioned plasmids. The cells were lysed in lysis buffer (140 mM NaCl, 3 mM KCl, 8 mM Na_2HPO_4, 1.5 mM KH_2PO_4, 0.2% Triton X-100, 2 mM EDTA, 2 mM EGTA) containing protease inhibitors (complete; Roche, Rotkreuz, Switzerland) and phosphatase inhibitors (Phosphostop, Roche). The lysates were cleared by centrifugation (20,000 x g, 4 °C, 10 min). Proteins were precipitated using Anti-FLAG M2 Magnetic Beads (Sigma-Aldrich) [51] and eluted from the beads using 0.1 M Glycin (pH 2,5). The eluate was neutralized with 1 M Tris (pH 10,6) and incubated with Laemmli sample buffer for 8 minutes at 95 °C. Flag-tagged AKAPs, RIα, RIIα and RIIβ were detected by Western blotting with specific primary and horseradish-coupled secondary antibodies (anti-Flag antibody: Sigma Aldrich #Flag M2; anti-RIα: BD Biosciences #610610, anti-RIIα: BD Biosciences #612243, anti-RIIβ: BD Biosciences #610626, anti-DDK (Flag): Origene TA50011, POD-anti-Mouse IgG: Immuno Research # 715-035-151) [10, 19].

Peptide spot array assay

Peptides derived from the AKB of AKAP18β were generated by automatic SPOT synthesis on Whatman 50 cellulose membranes using Fmoc (9-fluorenylmethyloxycarbonyl) chemistry and the Autospot-Robot ASS 222 (Intavis Bioanalytical Instruments, Köln, Germany). The interaction of membrane-bound peptides with RIIα was investigated by RII overlay. The membrane-bound peptides were overlaid with recombinant radioactively labelled RIIα subunits (^{32}P) as described previously [19, 35, 52]. Interaction was detected by autoradiography.

ACCESSION NUMBERS

Coordinates and structure factors for the human AKAP18β:RIIα-D/D have been deposited in the Protein Data Bank under accession code 4ZP3.

RESULTS AND DISCUSSION

Overall structure and crystal packing of AKAP18β:RIIα-D/D complex

AKAP18β (amino acid residues 43-83) and the D/D domain of RIIα (amino acid residues 1-44) were co-expressed in *E. coli* and the AKAP18β:RIIα-D/D complex purified. Its structure was determined by molecular replacement from a crystal diffracting to 2.63 Å resolution, and refined to a R_{work} and R_{free} of 22.2 % and 26.8 %, respectively (Table 1).

The asymmetric unit in the crystals contained six AKAP18β:RIIα-D/D complexes. Each complex is composed of one AKAP18β molecule bound to an RIIα-D/D dimer. The six AKAP18β:RIIα-D/D complexes are arranged as two identical pseudo-trimers in a propeller-like fashion (Supplementary Figure 2A). The central pseudo-threefold propeller axis is defined by two cadmium ions bound to Glu41 of the helices B and B' of all RIIα-D/D dimers (Supplementary Figure 2B). The pseudo-trimeric arrangement is further stabilised by two symmetric salt bridges between Arg38 and Glu34 of two adjacent D/D dimers (Supplementary Figure 2C). In each pseudo-trimer, the threefold symmetry is broken by one complex which is rotated 180° with respect to the two others, so that its bound AKAP18β extends into the opposite direction. However, the binding mode of AKAP18β to the RIIα-D/D dimer in the rotated complex is identical to the other two complexes. Overall, the superimposition of all six complex structures, found in the asymmetric unit of the crystal, revealed no major structural differences except for some termini in the molecules (see below). The six complexes align with averaged root-mean-square deviations (rmsd) between equivalent C_α atoms ranging from 0.330 to 0.318 Å.

Static light scattering coupled to size exclusion chromatography (SEC) and analytical ultracentrifugation was performed to investigate a putative physiological relevance of the bound cadmium ion in formation of higher oligomeric AKAP18β:RIIα-D/D complex structures. Both data sets show that the AKAP18β:RIIα-D/D complex has an absolute molecular mass between 13 and 17 kDa in the presence or absence of 2 mM $CdCl_2$ or 2 mM EDTA which is in agreement with the calculated molecular mass of 15 kDa of the AKAP18β:RIIα-D/D (1:2 molar ratio) complex (Supplementary Figure 3). No formation of higher oligomeric AKAP18β:RIIα-D/D complexes was observed, which indicates that cadmium only mediates the packing of AKAP18β:RIIα-D/D complexes in the crystal and does not have a biological relevance for this complex. Only in the presence of cadmium were crystals of the AKAP18β:RIIα-D/D complex obtained which diffracted to a suitable resolution for structure determination.

In two D/D complexes, the two N' termini are well ordered and positioned along the AKAP18β helix, as in the AKAP-*IS*:RIIα-D/D complex [18]. In the remaining four complexes, the N termini point ~90° away from the amphipathic helix and are less well ordered (Supplementary Figure 3). In addition, AKAP18β in all complexes varies at the N and C termini. The first 5 to 8 N-terminal residues and the last 3 to 8 C-terminal residues are disordered in the various molecules (Supplementary Figure 4B).

The hydrophobic core region is stabilised by flanking salt bridges

For a detailed description of the structure, two AKAP18β:RIIα-D/D complexes were superimposed with a rmsd of 0.305 Å to derive a model with the maximum length of the AKAP18β amphipathic helix in N- and C-terminal directions from amino acid position 48 to 80 (Figure 1). The RIIα-D/D dimer shows the known X-type helix bundle formed by the helices A, B, A' and B' (Figure 1A) [15-18]. The hydrophobic face of the amphipathic AKAP18β helix is composed of nine turns (I-IX) and docks into the hydrophobic cavity of the RIIα-D/D dimer, formed by helices A and A' of the two protomers of the D/D domains (Figures 1B and 2). Helix B and B' are not involved in the interaction (Figure 1A). AKAP18β shows an asymmetric

binding to the RIIα-D/D dimer (Figure 2) as also observed for AKAP-*IS* and D-AKAP2 [17, 18]. Our complex structure indicates that the asymmetric orientation of the AKAP helix is governed by the localization of the conserved hydrophobic core sequence for RII binding *H*xx*HH*xx*HH*xx*HH*xx*HH* of the amphipathic helix and is not caused by crystal contacts or by a flexible N' tail of the RIIα-D/D dimer as assumed for the AKAP-*IS* and D-AKAP2 complex structures [17, 18].

11 residues in the AKAP18β helix (Leu52, Val53, Leu55, Leu59, Val60, Ala63, Val64, Ala67, Val68, Tyr71 and Leu72) engage in hydrophobic interactions with the RIIα-D/D dimer (Figure 1B and 2A). The amphipathic hydrophobic core is localized within turns I to VI of the AKAP18β helix and constitutes the backbone of the interaction. In addition, Leu52, Leu55, Leu59, Val68, Tyr71 and Leu72 project horizontally along the D/D dimer and mediate binding to a hydrophobic surface in the RIIα-D/D N termini. Of note, Asp49 and Glu74 are engaged in salt bridges with Arg22 and Arg22' located in the RIIα-D/D helices A and A', respectively (Figure 2A). The binding of the C terminus of the AKAP helix to the RIIα-D/D dimer is further stabilized by an H-bond formed by AKAP18β Gln70 with Gln14 of the RIIα-D/D dimer. This polar interaction was also observed in the binding of AKAP-*IS* to the RIIα-D/D dimer [18]. A schematic representation of the interactions is shown in Figure 2B.

Anchor points in AKAP helices define specificity for PKA binding

Surprisingly, two additional polar interactions of Arg22' and Arg22 of the RIIα-D/D dimer with the AKAP18β residues Asp49 and Glu74, respectively, were observed. In addition, Gln14 of the RIIα helix A forms a hydrogen bond with AKAP18β residue Gln70. Thus Asp49, Gln70 and Glu74 appear to serve as hydrophilic anchors in the long AKAP helix to facilitate a stable and specific binding to RIIα-D/D dimers (see below). This set of three additional interactions was not found in the so far known AKAP:RIIα-D/D dimer complex structures due to the limited lengths of the bound AKAP helices (17-24 amino acids) compared with the long AKAP18β helix reported here (32 residues).

Besides the five conserved hydrophobic core patches (Figure 2B), the three additional anchor points support the orientation of the AKAP helix relative to the RIIα-D/D dimer. The long straight AKAP18β helix is bound with an angle of 44° to the RIIα N-terminal helix A (Figure 3A). Sequence alignment of RI-, RII- and dual-specific AKAPs revealed a conservation of the three anchor points for RII binding AKAPs (Figure 3E). Analyses of the structurally known complexes of RIIα-D/D bound to AKAP79 (AKAP5) and to D-AKAP2 (AKAP10) revealed a similar binding angle for the AKAP helix of 46° and 47°, respectively (Figure 3B, D). We assume that AKAPs with either an Asp or Glu in anchor point position I and III in the helix, bind with an angle between 44° and 47° to the RIIα helix A. The distance of the C_α atoms of anchor points I and III is 37 Å spanning 25 residues. This supports a rigid binding mode for RII-specific AKAPs because the RIIα D/D dimer presents two Arg22 residues, which are the counterparts for salt bridge formation with anchor points I and III (Figure 3A). Gln14 in the RIIα-D/D dimer constitutes the binding site for anchor point II and allows for a greater variety of interacting amino acids in the AKAP helix, like Gln, Asn, Glu, Asp, Lys and Arg. These residues have the potential to engage in hydrogen bonds with Gln14 to further stabilize the AKAP:RIIα-D/D interaction.

Based on sequence alignments, we expect that the RII-specific AKAP18α, AKAP18δ, AKAP6 and AKAP14 bind in a similar fashion to RII (Figure 3E), because they contain the same three anchor points. RII-specific AKAPs which do not have the conserved anchor point residues may adopt a more flexible binding mode, giving the freedom for bending of the AKAP helix such as seen in the AKAP13 (AKAP-Lbc):RIIα-D/D complex (Figure 3C). The bent AKAP-Lbc helix binds with an angle of approximately 29° to the RIIα helix A. A similar binding behaviour is expected for the RII-specific AKAP8, AKAP9, AKAP12 and GSKIP as they are also lacking the three required anchor point residues. This shows that two different bind-

ing modes to RIIα exist. Even more important, the three identified anchor points are not only involved in orienting the AKAP helix with regard to the RIIα-D/D domain, but they further define the binding frame for RII-specific AKAPs (Figure 3A, E). The previously known five hydrophobic patches of the amphipathic AKAP helix (Figure 3B) are now flanked by the three anchor points in the fashion ***N***xx*H*xx*HH*xx*HH*xx*HH*xx*HH*x***P***xx***N***, where *N* stands for negatively charged, *H* for hydrophobic, *P* for polar and x for any residue. Sequence alignments reveal that also the dual-specific AKAP5, AKAP10 (D-AKAP2), Ezrin, AKAP1, and MAP2D may bind RIIα in a similar fashion as observed for AKAP18β (Figure 3A) in our structure (Figure 3E). Only AKAP4 (FSC1A) and AKAP11 of the dual-specific AKAPs lack all, and AKAP3 one of the anchor points. These AKAPs are probably more flexible in binding to RIIα, as also seen for AKAP13.

On closer inspection of the structures of the dual specific D-AKAP2 bound to RIα (PDB: 3IM4) and RIIα (PDB: 2HWN), together with sequence alignment analyses, it also becomes evident that a RIα-specific anchor frame exists, which differs from the RIIα anchor frame (Figure 3D, E). The AKAP RIα anchor frame follows the sequence pattern ***N***x*HH*xx*HH*xx*HH*x***P***HHx***N***H*. The RIα anchor point II is inserted between hydrophobic patches 3 and 4 and anchor III between patches 4 and 5 (Figure 3E). This is in contrast to the RIIα anchor points II and III, which are located C-terminally after patch 5. The central hydrophobic core patch in the AKAP sequence makes a helical register shift of one turn in the C-terminal direction, compared to the RIIα frame. The shift was already reported in the comparison of the two D-AKAP2 complex structures [53]. We observe that RIα anchor point III is placed by the helical shift to the same local position of anchor point II in the RIIα bound AKAPs (Figure 3E). However, because the D-AKAP2 helix in the RIIα-D/D domain bound complex is too short, the two different anchor frames for RIα and RIIα were not recognized. The two specific frames at the AKAP helix, together with the complementing amino acids in the D/D domains, become visible upon superimposition of the D-AKAP2:RIα and D-AKAP2:RIIα complex structures (Figure 3D). In the D-AKAP2:RIα complex anchor points I (Glu632) and III (Gln649) bind to the complementary positively charged Lys30 residues in the RIα-D/D dimer. This is comparable with anchor points I and III in RIIα-specific AKAPs which bind the complementary Arg22 residues in the RIIα-D/D dimer, but with the difference that the RIα-specific anchor points I and II have a closer C_α distance of 25 Å to each other, as seen for RIIα with 30 Å.

Sequence alignments indicate that the need of all three anchor points in the AKAP helix for specific binding to RIα may not be as crucial as for binding to RIIα (Figure 3E). The AKAPs specific for RIα often use only a set of two anchor points in different combinations as observed for $AKAP_{CE}$, smAKAP, SKIP and PAP7. The same is recognized for most of the dual-specific AKAPs aligned in frame for RIα binding, like AKAP5, Ezrin, AKAP4 (FSC1A), AKAP11 and MAD2D with the exception of AKAP10 (D-AKAP2) and AKAP1, which make use of three anchor points. AKAP3 and AKAP4 (FSC1B) employ only the most highly conserved anchor point II for RIα binding, suggesting a slightly different binding compared to D-AKAP2 binding of RIα.

Loss of anchor points in AKAP18 crucially reduces RII binding *in vitro*

In order to evaluate the influence of individual amino acids on the interaction between AKAP18β and full-length RIIα subunits of PKA, we substituted each amino acid residue between D49 and E74 of AKAP18β with alanine. 30mer peptides representing the wild-type sequence or peptides carrying the substitutions were spot-synthesized and overlaid with radioactively labelled RIIα subunits (Figure 4). Substitutions of any of the amino acid residues engaged in hydrophobic interactions with an alanine did not substantially affect the binding. Binding was reduced by a maximum of 25 %, for example by L59A (Figure 4A). Only the introduction of kinks into the helix by substitution of two hydrophobic amino acid residues with prolines abolished the binding (Figure 4A). Individual alanine substitutions of the anchor points D49, Q70 and E74 modestly reduced the binding. However, if two of these anchors were replaced by alanine, the binding decreased by approximately 60 %. Moreover, the loss

of all three amino acid residues reduced binding to 40 % compared to the interaction of the wild-type sequence (Figure 4B). Thus these three residues are key determinants of the AKAP18β-RIIα interaction. We also substituted amino acids between D49 and E74 individually with Asp and carried out an RII overlay (Figure 4C). The introduction of the negative charge had generally more pronounced effects on the interaction compared to the Ala substitutions. Replacement of S56, L59, V60, A63, V64 or A67 reduced binding by at least 60 %. A reduction by approximately 40 % resulted from substitutions of the hydrophobic residues L52, L55 or V68 with Asp, which are involved in the binding of the N termini of the RIIα-D/D domain. The single substitutions of anchor points II (Q70) and III (E74) with the negatively charged Asp or with Ala alone, hardly affected the interaction (Figure 4B, C). These experiments confirm that substitution of an individual anchor point either with an Ala or an Asp does not effectively interfere with the interaction, i.e. a minimum of two anchor points are sufficient to maintain a stable AKAP:RIIα interaction.

To estimate the relative binding affinity of the triple-Ala-AKAP18β (D49A/Q70A/E74A) to the D/D domain of PKA in comparison to the wild type AKAP18β, an *in silico* approach using the Prime/MM-GBSA module of the Schrödinger suite [54] was used to calculate the free energy of binding ΔG_{bind} (kJ/mol). For the AKAP18β-wt:RIIα-D/D complex the calculation of ΔG_{bind} resulted in -179.9 kJ/mol, whereas the loss of three bonds in the triple-Ala-AKAP18β led to a decreased ΔG_{bind} free binding energy of -167.6 kJ/mol. From these values the calculated K_D of triple-Ala-AKAP18β is 140-fold larger than the K_D of AKAP18β. This supports computationally the reduction in binding affinity of triple-Ala-AKAP18β and together with the peptide spot analyses confirms the importance of the hydrophilic anchor point interactions of AKAP18β and the RIIα-D/D domain.
ITC measurements were performed to evaluate the binding strength of AKAP18β(43-83) and the triple anchor point substitution AKAP18β(43-83)D49A/Q70A/E74A. One AKAP18β(43-83) molecule binds to one RIIα-D/D dimer with an estimated dissociation constant of K_D = 0.6 nM ± 0.2 nM using a one-site binding model (Figure 5A). This value is close to K_D values determined in Biacore measurements for the interaction of a peptide (25mer) representing the PKA binding domain of AKAP18δ to RIIα (0.4 nM) [10, 35]. Binding of AKAP18β(43-83)D49A/Q70A/E74A to the D/D domain was dramatically different. The titration could only be fitted with a sequential binding model and allowed an estimation of the binding constants for the two binding phases of K_{D1}= 0.4 nM and K_{D2} = 22.8 nM (Figure 5A). Presumably, the AKAP18β(43-83)D49A/Q70A/E74A helix cannot immediately anchor to the D/D domain, resulting in multiple different binding modi. These observations underline our findings in the peptide spot analyses and the *in silico* calculations that, as soon as AKAP18β lacks two or three anchor points, a drastic reduction of binding strength to the RIIα-D/D dimer results.
To determine the kinetics for the interaction of RIIα with wild type AKAP18β(43-83) and the triple mutant, surface plasmon resonance measurements were performed. RIIα was captured on an 8-AHA-cAMP chip and the AKAP18β variants were injected at a flow rate of 100 µl/min. For the association, the AKAP18 variants were injected for 60 s. Both variants displayed similar association behaviours (Figure 5B, insert). To obtain accurate dissociation phases, the dissociation phases were recorded for 2 h and dissociation rate constants of $3.1 \cdot 10^{-5}$ $mol^{-}1s^{-1}$ and $1.5 \cdot 10^{-4}$ $mol^{-}1s^{-1}$ were calculated for wild type and mutant protein, respectively. A 10-fold faster dissociation rate of the triple mutant compared to the wild type was revealed (Figure 5B). Thus it appears that the anchor points affect the dissociation of AKAP18 from rather than the association with RIIα.

Loss of anchor points in AKAP18γ and smAKAP reduces binding of regulatory subunits of PKA in cells

Next, we examined whether the loss of anchor points affects the interaction of a full-length AKAP18 with RII subunits in cells. AKAP18γ, which encompasses the region of AKAP18β that was co-crystallised with the DD domain of RIIα, and which is longer than AKAP18β (326 *vs.* 104 amino acids) was expressed in HEK293 cells as a Flag-tagged protein. The Flag-tagged AKAP18γ was immunoprecipitated with anti-Flag magnetic beads and co-

immunoprecipitated RIIα and RIIβ were detected by Western blotting (Figure 6A). The anchor point substitutions in AKAP18γ(D293A/Q314A/E318A) correspond to the ones in AKAP18β (D49A/Q70A/E74A). These substitutions reduced the interactions of AKAP18γ with both RII subunits, whereby the interaction with RIIβ was more strongly affected than the one with RIIα.
As an example for a full-length RI-specific AKAP, we examined whether the loss of the predicted anchor points in smAKAP (Figure 3E) affects its interaction with RIα subunits (Figure 6B). Indeed, co-immunoprecipitation studies confirmed that the interaction of smAKAP carrying Ala in the anchor point positions (D72A/Q76A) with RIα is strongly reduced compared to the interaction of the wild type smAKAP with RIα.

Conclusions

Our current analyses are in line with our previous study of the AKAP18δ-RIIα interaction where we used molecular modelling in combination with RII overlays over 25mer peptides that covered the RII-binding domain of AKAP18δ [35, 43]. These studies had defined six hydrophobic interactions (Leu52, Leu59, Val60, Ala63, Val64 and Ala67 of AKAP18β). The core PKA-binding domains of the rat AKAP18δ and the human AKAP18α, β and γ are identical in sequence. Thus the new complex structure presumably represents the PKA-binding mode of all AKAP18 isoforms. Our previous analysis of interactions of AKAP18δ with membrane lipids identified clusters of positively charged amino acids on the surface of the molecule that can interact with negatively charged lipids [55]. In addition, a recent modelling study suggested a pentameric organisation of AKAP18γ in complex with two RII and two C subunits of PKA [56]. Furthermore, a 3D structure of around 200 amino acids N-terminally from the RII-binding domain of AKAP18γ is available [57]. Thus a picture of the AKAP18 structure is emerging. However, a full-length 3D structure of any of the AKAP18 isoforms with full-length RII subunits of PKA is lacking.

In summary, the novel AKAP18β:RIIα-D/D complex structure exhibits pivotal hydrophilic anchor points important for recognition of PKA RII subtypes that were hitherto unknown. Targeting these amino acid residues can lower the binding affinity or prevent the interaction. Thus, these anchor points provide a unique opportunity for specific pharmacological interference and may act as the basis for the design of specific inhibitors that will permit ascribing functions to this specific AKAP-PKA interaction. Our sequence alignments and biochemical analyses suggest the presence of different sets of anchor points in different AKAPs. These anchor points may generally influence the binding affinity between AKAPs and R subunits of PKA and may thus lead to new strategies for pharmacological targeting also of other AKAP-PKA interactions. This is so far not possible as only global disruptors of AKAP-PKA interactions are available [4].

ACKNOWLEDGEMENTS

This work was supported by grants from the Else Kröner-Fresenius-Stiftung (2013_A145), the German-Israeli Foundation (I-1210-286.13/2012), the Deutsche Forschungsgemeinschaft (DFG, KL1415/4-2) and the German Centre for Cardiovascular Research (DZHK 81X210012) to EK, and by the DFG (1818/6) to FWH. We thank Verena Ezerski for technical help in generating AKAP18β constructs and Eva Rosenbaum for advice concerning analytical ultracentrifugation. We also thank Oxana Krylova for her support in isothermal titration calorimetry experiments.

Author Contributions

FG generated recombinant proteins, carried out fine screens for crystallography, ITC, SLS and analytical ultracentrifugation; YR collected data at Bessy II, determined the structure and contributed to writing the manuscript; MS generated Flag-tagged AKAP constructs and cAMP-agarose and immunoprecipitations, KF participated in the design of experiments; KeZ synthesized and analysed peptide spots; AK and GK estimated *in silico* binding energies; KA and FWH provided PKA constructs, performed Biacore experiments; OD and UH advised on protein expression and crystallization trials; YR, FG and EK designed experiments and wrote the manuscript.

Table 1 - Data collection and refinement statistics

	AKAP18β:RIIα-D/D
Data collection	
Beamline	BESSY 14.1
Wavelength (Å)	0.9184
Space group	$P2_1$
Cell dimensions	
a, *b*, *c* (Å)	56.9, 121.0, 57.1
α, β,γ (°)	90.0, 93.1, 90.0
Resolution (Å)*	41.5-2.63 (2.79-2.63)
R_{meas}* (%)	13.0 (58.2)
$< I / \sigma(I) >$*	10.6 (2.5)
Completeness (%)*	99.4 (99.0)
Redundancy*	3.2
Refinement	
Resolution (Å)	2.63
No. reflections	21,760
R_{work} / R_{free}	0.222 / 0.268
No. atoms	
Protein	5,319
Ligand/ion	6
Water	60
Mean *B* factor (Å^2)	36.8
R.m.s deviations	
Bond lengths (Å)	0.007
Bond angles (°)	1.120

*Data in highest resolution shell are indicated in parentheses.

Figure Legends

Figure 1. **Model of the D/D domain of human regulatory RIIα subunits of PKA bound to the A-kinase binding domain (AKB) of AKAP18β**
(A) The X-type four helix bundle of the RIIα D/D dimer is composed of helices A, B and A', B' coloured in blue and salmon, respectively. Two AKAP18β:RIIα-D/D complexes involving chains I, J and G,H for RIIα-D/D with the corresponding AKAP18β helices chains Q and P, respectively, were superimposed to derive a model with the maximum length of AKAP18β (coloured in yellow). For clarity only chains G and H of RIIα-D/D in combination with AKAP18β helix chains Q and P are shown. The side view along the AKAP18β helix demonstrates the binding of AKAP18β by the helices A and A' of RIIα-D/D dimer.
(B) Surface representation of the hydrophobic cavity of the RIIα-D/D dimer with the bound AKAP18β helix shown in yellow. Hydrophobic residues of the RIIα-D/D dimer are shown in grey colour, polar residues in green, negatively and positively charged residues in red and blue, respectively.

Figure 2. Detailed presentation of the binding of AKAP18β to a RIIα-D/D dimer
(A) Two-side view of the AKAP18β:RIIα-D/D binding interface. The nine turns (I-IX) of the AKAP18β amphipathic helix (yellow) bind with their hydrophobic sides to the helices A and A' (blue and salmon, respectively) of the RIIα-D/D dimer. Beside the hydrophobic core region crucial additional salt bridges (dotted lines) stabilize the interface. Only the residues involved in complex formation are shown.
(B) Schematic presentation of the binding interface between AKAP18β and a RIIα-D/D dimer. Solid and dashed lines describe the polar and the hydrophobic interactions, respectively. The conserved hydrophobic patches are indicated as grey boxes and numbered from N- to C-terminus.

Figure 3. AKAP anchor points I-III for interaction with D/D domains of regulatory subunits of PKA. The monomers of the RIIα-D/D dimer are depicted in blue and salmon cartoons and the AKAP helices as ribbons. The anchor points in the AKAP helices, specific for RIα and RIIα binding, are shown as yellow and red spheres, respectively. The complementary anchor points at the D/D domains are displayed as green and blue spheres for RIα and RIIα, respectively.
(A) The AKAP18β helix containing the three anchor points, bound to RIIα-D/D, is shown in yellow. The short AKAP79 (AKAP5) with one anchor point is shown in
(B) and the longer AKAP-Lbc (AKAP13) with no anchor points is presented in
(C), both in grey colour.
(D) Superimposition of D-AKAP2 (AKAP10) depicted as grey ribbon in complex with RIIα-D/D (blue and salmon) onto the complex of D-AKAP2 (black ribbon) bound to RIα-D/D (green cartoon). The approximate position of anchor points II and III for the D-AKAP2:RIIα-D/D complex are modelled onto the D-AKAP2 helix of the D-AKAP2:RIIα-D/D complex. The positions were estimated based on the observed locations in AKAP18β and on the sequence alignment shown in E.
(E) Alignment of the PKA-binding domains and adjacent sequences of the indicated AKAPs. The five conserved hydrophobic patches forming the core of the interactions between AKAPs and D/D domains are depicted as grey boxes. Amino acid residues matching the hydrophobic core are emphasized in bold letters. The anchor point positions I, II and III, specific for RIα and RIIα binding are marked with yellow and red boxes, respectively. AKAP18β residues involved in RIIα binding are highlighted with an asterisk. The dual specificity AKAPs are aligned either to the RI or to the RII binding frame.

Figure 4. Hydrophilic anchor points are essential for the interaction of AKAP18β with regulatory RIIα subunits of PKA and hydrophobic bonds constitute the backbone. 30mer peptides representing the wild-type sequence of the PKA-binding domain of AKAP18β and peptides with

(A) individual Ala substitutions,
(B) combinations of Ala substitutions or
(C) individual Asp (D) substitutions in the indicated positions were spot-synthesized and overlaid with radioactively labelled RIIα subunits. Binding of RIIα to the peptides was detected by autoradiography. In positions 50, 63 and 67 the wild-type sequence contains Ala, and therefore shown only once in A. Representative spots from three independent experiments are shown. Quantification in B represents the mean ± S.E. from three independent experiments. For statistical analyses the Student's unpaired t-test was applied.

Figure 5. Substitution of the anchor points in AKAP18β reduces the binding affinity and increases the dissociation rate from RIIα.
(A) The upper panels show the raw ITC data and the bottom panels show the change in molar heat as a function of the molar ratio of wild type AKAP18β(43-83) and AKAP18β(43-83/D49A/Q70A/E74A) to RIIα-D/D(1-44) (left and right panels, respectively). The data of three independent measurements were fitted with the one set of sites model and yielded a mean dissociation constant of K_D = 0.6 ± 0.2 nM, N = 0.98 sites, ΔH = -2.255E4 ± 171.2 cal/mol, ΔS = -33.4 cal/mol/deg for the wild type protein. A fit for the ITC data for AKAP18β(43-83/D49A/Q70A/E74A) was only possible with an sequential binding model; dissociation constants for the two binding phases were estimated from 4 independent experiments to be K_{D1}= 0.4 nM and K_{D2}= 22.8 nM.
(B) Surface plasmon resonance (SPR) analysis of the interaction of RIIα subunit and AKAP18β. 290 resonance units (RU) of RIIα were captured on an 8-AHA cAMP sensor chip. Wild type AKAP18β(43-83) (black lines) and the AKAP18β triple mutant (blue lines) were injected in concentrations ranging from 0.2 nM-146 nM. The association phases of the peptides (0.2 nM – 49 nM) were monitored for 60 s illustrated in the insert. The dissociation phase of the highest concentration tested (146 nM) was monitored for 2 h and separately fitted to determine the dissociation rate (red dashed lines).

Figure 6. The loss of the anchor points in full-length AKAP18γ and the RI-specific smAKAP decreases interactions with R subunits of PKA in cells.
(A-B) The indicated Flag-tagged full-length wild type AKAPs (WT) and the variants lacking the anchor points and were expressed in HEK293 cells. AKAP18γ lacks the anchor points for RII (AAA) and smAKAP for RI (AA) subunits. The AKAPs were immunoprecipitated (IP) with anti-Flag magnetic beads. The AKAPs and R subunits were detected by Western blotting (IB) using anti-Flag, anti-RIα, anti RIIα and anti-RIIβ antibodies. For statistical analyses the Student's t-test was applied.

References

1 Skroblin, P., Grossmann, S., Schafer, G., Rosenthal, W. and Klussmann, E. (2010) Mechanisms of protein kinase a anchoring. Int Rev Cell Mol Biol. **283**, 235-330

2 Scott, J. D., Dessauer, C. W. and Tasken, K. (2013) Creating order from chaos: cellular regulation by kinase anchoring. Annual review of pharmacology and toxicology. **53**, 187-210

3 Troger, J., Moutty, M. C., Skroblin, P. and Klussmann, E. (2012) A-kinase anchoring proteins as potential drug targets. British journal of pharmacology. **166**, 420-433

4 Dema, A., Perets, E., Schulz, M. S., Deak, V. A. and Klussmann, E. (2015) Pharmacological targeting of AKAP-directed compartmentalized cAMP signalling. Cell Signal. **27**, 2474-2487

5 Langeberg, L. K. and Scott, J. D. (2015) Signalling scaffolds and local organization of cellular behaviour. Nat Rev Mol Cell Biol. **16**, 232-244

6 Klussmann, E. (2015) Protein-protein interactions of PDE4 family members - Functions, interactions and therapeutic value. Cell Signal

7 Taylor, S. S., Ilouz, R., Zhang, P. and Kornev, A. P. (2012) Assembly of allosteric macromolecular switches: lessons from PKA. Nat Rev Mol Cell Biol. **13**, 646-658

8 Huang, L. J., Durick, K., Weiner, J. A., Chun, J. and Taylor, S. S. (1997) D-AKAP2, a novel protein kinase A anchoring protein with a putative RGS domain. Proc Natl Acad Sci U S A. **94**, 11184-11189

9 Huang, L. J., Durick, K., Weiner, J. A., Chun, J. and Taylor, S. S. (1997) Identification of a novel protein kinase A anchoring protein that binds both type I and type II regulatory subunits. J Biol Chem. **272**, 8057-8064

10 Henn, V., Edemir, B., Stefan, E., Wiesner, B., Lorenz, D., Theilig, F., Schmitt, R., Vossebein, L., Tamma, G., Beyermann, M., Krause, E., Herberg, F. W., Valenti, G., Bachmann, S., Rosenthal, W. and Klussmann, E. (2004) Identification of a novel A-kinase anchoring protein 18 isoform and evidence for its role in the vasopressin-induced aquaporin-2 shuttle in renal principal cells. J Biol Chem. **279**, 26654-26665

11 McSorley, T., Stefan, E., Henn, V., Wiesner, B., Baillie, G. S., Houslay, M. D., Rosenthal, W. and Klussmann, E. (2006) Spatial organisation of AKAP18 and PDE4 isoforms in renal collecting duct principal cells. European journal of cell biology. **85**, 673-678

12 Means, C. K., Lygren, B., Langeberg, L. K., Jain, A., Dixon, R. E., Vega, A. L., Gold, M. G., Petrosyan, S., Taylor, S. S., Murphy, A. N., Ha, T., Santana, L. F., Tasken, K. and Scott, J. D. (2011) An entirely specific type I A-kinase anchoring protein that can sequester two molecules of protein kinase A at mitochondria. Proc Natl Acad Sci U S A. **108**, E1227-1235

13 Kovanich, D., van der Heyden, M. A., Aye, T. T., van Veen, T. A., Heck, A. J. and Scholten, A. (2010) Sphingosine kinase interacting protein is an A-kinase anchoring protein specific for type I cAMP-dependent protein kinase. Chembiochem : a European journal of chemical biology. **11**, 963-971

14 Burgers, P. P., Ma, Y., Margarucci, L., Mackey, M., van der Heyden, M. A., Ellisman, M., Scholten, A., Taylor, S. S. and Heck, A. J. (2012) A small novel A-kinase anchoring protein (AKAP) that localizes specifically protein kinase A-regulatory subunit I (PKA-RI) to the plasma membrane. J Biol Chem. **287**, 43789-43797

15 Newlon, M. G., Roy, M., Morikis, D., Hausken, Z. E., Coghlan, V., Scott, J. D. and Jennings, P. A. (1999) The molecular basis for protein kinase A anchoring revealed by solution NMR. Nat Struct Biol. **6**, 222-227

16 Newlon, M. G., Roy, M., Morikis, D., Carr, D. W., Westphal, R., Scott, J. D. and Jennings, P. A. (2001) A novel mechanism of PKA anchoring revealed by solution structures of anchoring complexes. EMBO J. **20**, 1651-1662

17 Kinderman, F. S., Kim, C., von Daake, S., Ma, Y., Pham, B. Q., Spraggon, G., Xuong, N. H., Jennings, P. A. and Taylor, S. S. (2006) A dynamic mechanism for AKAP binding to RII isoforms of cAMP-dependent protein kinase. Mol Cell. **24**, 397-408

18 Gold, M. G., Lygren, B., Dokurno, P., Hoshi, N., McConnachie, G., Tasken, K., Carlson, C. R., Scott, J. D. and Barford, D. (2006) Molecular basis of AKAP specificity for PKA regulatory subunits. Mol Cell. **24**, 383-395
19 Hundsrucker, C., Skroblin, P., Christian, F., Zenn, H. M., Popara, V., Joshi, M., Eichhorst, J., Wiesner, B., Herberg, F. W., Reif, B., Rosenthal, W. and Klussmann, E. (2010) Glycogen synthase kinase 3beta interaction protein functions as an A-kinase anchoring protein. J Biol Chem. **285**, 5507-5521
20 Burgers, P. P., van der Heyden, M. A., Kok, B., Heck, A. J. and Scholten, A. (2015) A systematic evaluation of protein kinase a-a-kinase anchoring protein interaction motifs. Biochemistry. **54**, 11-21
21 Jarnaess, E., Ruppelt, A., Stokka, A. J., Lygren, B., Scott, J. D. and Tasken, K. (2008) Dual specificity A-kinase anchoring proteins (AKAPs) contain an additional binding region that enhances targeting of protein kinase A type I. J Biol Chem. **283**, 33708-33718
22 Christian, F., Szaszak, M., Friedl, S., Drewianka, S., Lorenz, D., Goncalves, A., Furkert, J., Vargas, C., Schmieder, P., Gotz, F., Zuhlke, K., Moutty, M., Gottert, H., Joshi, M., Reif, B., Haase, H., Morano, I., Grossmann, S., Klukovits, A., Verli, J., Gaspar, R., Noack, C., Bergmann, M., Kass, R., Hampel, K., Kashin, D., Genieser, H. G., Herberg, F. W., Willoughby, D., Cooper, D. M., Baillie, G. S., Houslay, M. D., von Kries, J. P., Zimmermann, B., Rosenthal, W. and Klussmann, E. (2011) Small molecule AKAP-protein kinase A (PKA) interaction disruptors that activate PKA interfere with compartmentalized cAMP signaling in cardiac myocytes. The Journal of biological chemistry. **286**, 9079-9096
23 Klussmann, E., Maric, K., Wiesner, B., Beyermann, M. and Rosenthal, W. (1999) Protein kinase A anchoring proteins are required for vasopressin-mediated translocation of aquaporin-2 into cell membranes of renal principal cells. J Biol Chem. **274**, 4934-4938
24 Klussmann, E. and Rosenthal, W. (2001) Role and identification of protein kinase A anchoring proteins in vasopressin-mediated aquaporin-2 translocation. Kidney Int. **60**, 446-449
25 Diviani, D., Dodge-Kafka, K. L., Li, J. and Kapiloff, M. S. (2011) A-kinase anchoring proteins: scaffolding proteins in the heart. Am J Physiol Heart Circ Physiol. **301**, H1742-1753
26 Pidoux, G., Witczak, O., Jarnaess, E., Myrvold, L., Urlaub, H., Stokka, A. J., Kuntziger, T. and Tasken, K. (2011) Optic atrophy 1 is an A-kinase anchoring protein on lipid droplets that mediates adrenergic control of lipolysis. The EMBO journal. **30**, 4371-4386
27 Szaszak, M., Christian, F., Rosenthal, W. and Klussmann, E. (2008) Compartmentalized cAMP signalling in regulated exocytic processes in non-neuronal cells. Cell Signal. **20**, 590-601
28 Henn, V., Stefan, E., Baillie, G. S., Houslay, M. D., Rosenthal, W. and Klussmann, E. (2005) Compartmentalized cAMP signalling regulates vasopressin-mediated water reabsorption by controlling aquaporin-2. Biochem Soc Trans. **33**, 1316-1318
29 Fraser, I. D., Tavalin, S. J., Lester, L. B., Langeberg, L. K., Westphal, A. M., Dean, R. A., Marrion, N. V. and Scott, J. D. (1998) A novel lipid-anchored A-kinase Anchoring Protein facilitates cAMP-responsive membrane events. EMBO J. **17**, 2261-2272
30 Trotter, K. W., Fraser, I. D., Scott, G. K., Stutts, M. J., Scott, J. D. and Milgram, S. L. (1999) Alternative splicing regulates the subcellular localization of A-kinase anchoring protein 18 isoforms. J Cell Biol. **147**, 1481-1492
31 Gray, P. C., Johnson, B. D., Westenbroek, R. E., Hays, L. G., Yates, J. R., 3rd, Scheuer, T., Catterall, W. A. and Murphy, B. J. (1998) Primary structure and function of an A kinase anchoring protein associated with calcium channels. Neuron. **20**, 1017-1026
32 Ahmad, F., Shen, W., Vandeput, F., Szabo-Fresnais, N., Krall, J., Degerman, E., Goetz, F., Klussmann, E., Movsesian, M. and Manganiello, V. (2015) Regulation of sarcoplasmic reticulum Ca2+ ATPase 2 (SERCA2) activity by phosphodiesterase 3A

(PDE3A) in human myocardium: phosphorylation-dependent interaction of PDE3A1 with SERCA2. J Biol Chem. **290**, 6763-6776
33 Lygren, B., Carlson, C. R., Santamaria, K., Lissandron, V., McSorley, T., Litzenberg, J., Lorenz, D., Wiesner, B., Rosenthal, W., Zaccolo, M., Tasken, K. and Klussmann, E. (2007) AKAP complex regulates Ca2+ re-uptake into heart sarcoplasmic reticulum. EMBO Rep. **8**, 1061-1067
34 Carr, D. W., Stofko-Hahn, R. E., Fraser, I. D., Bishop, S. M., Acott, T. S., Brennan, R. G. and Scott, J. D. (1991) Interaction of the regulatory subunit (RII) of cAMP-dependent protein kinase with RII-anchoring proteins occurs through an amphipathic helix binding motif. J Biol Chem. **266**, 14188-14192
35 Hundsrucker, C., Krause, G., Beyermann, M., Prinz, A., Zimmermann, B., Diekmann, O., Lorenz, D., Stefan, E., Nedvetsky, P., Dathe, M., Christian, F., McSorley, T., Krause, E., McConnachie, G., Herberg, F. W., Scott, J. D., Rosenthal, W. and Klussmann, E. (2006) High-affinity AKAP7delta-protein kinase A interaction yields novel protein kinase A-anchoring disruptor peptides. Biochem J. **396**, 297-306
36 Wang, Y., Ho, T. G., Bertinetti, D., Neddermann, M., Franz, E., Mo, G. C., Schendowich, L. P., Sukhu, A., Spelts, R. C., Zhang, J., Herberg, F. W. and Kennedy, E. J. (2014) Isoform-selective disruption of AKAP-localized PKA using hydrocarbon stapled peptides. ACS chemical biology. **9**, 635-642
37 Carlson, C. R., Lygren, B., Berge, T., Hoshi, N., Wong, W., Tasken, K. and Scott, J. D. (2006) Delineation of type I protein kinase A-selective signaling events using an RI anchoring disruptor. J Biol Chem. **281**, 21535-21545
38 Alto, N. M., Soderling, S. H., Hoshi, N., Langeberg, L. K., Fayos, R., Jennings, P. A. and Scott, J. D. (2003) Bioinformatic design of A-kinase anchoring protein-in silico: a potent and selective peptide antagonist of type II protein kinase A anchoring. Proc Natl Acad Sci U S A. **100**, 4445-4450
39 Burns-Hamuro, L. L., Ma, Y., Kammerer, S., Reineke, U., Self, C., Cook, C., Olson, G. L., Cantor, C. R., Braun, A. and Taylor, S. S. (2003) Designing isoform-specific peptide disruptors of protein kinase A localization. Proc Natl Acad Sci U S A. **100**, 4072-4077
40 Wang, Y., Ho, T. G., Franz, E., Hermann, J. S., Smith, F. D., Hehnly, H., Esseltine, J. L., Hanold, L. E., Murph, M. M., Bertinetti, D., Scott, J. D., Herberg, F. W. and Kennedy, E. J. (2015) PKA-Type I Selective Constrained Peptide Disruptors of AKAP Complexes. ACS chemical biology
41 Deak, V. A. and Klussmann, E. (2015) Pharmacological interference with protein-protein interactions of A-kinase anchoring proteins as a strategy for the treatment of disease. Curr Drug Targets
42 Gold, M. G., Fowler, D. M., Means, C. K., Pawson, C. T., Stephany, J. J., Langeberg, L. K., Fields, S. and Scott, J. D. (2013) Engineering A-kinase anchoring protein (AKAP)-selective regulatory subunits of protein kinase A (PKA) through structure-based phage selection. J Biol Chem. **288**, 17111-17121
43 Schafer, G., Milic, J., Eldahshan, A., Gotz, F., Zuhlke, K., Schillinger, C., Kreuchwig, A., Elkins, J. M., Abdul Azeez, K. R., Oder, A., Moutty, M. C., Masada, N., Beerbaum, M., Schlegel, B., Niquet, S., Schmieder, P., Krause, G., von Kries, J. P., Cooper, D. M., Knapp, S., Rademann, J., Rosenthal, W. and Klussmann, E. (2013) Highly functionalized terpyridines as competitive inhibitors of AKAP-PKA interactions. Angew Chem Int Ed Engl. **52**, 12187-12191
44 Krug, M., Weiss, M. S., Heinemann, U. and Mueller, U. (2012) XDSAPP: a graphical user interface for the convenient processing of diffraction data using XDS. Journal of Applied Crystallography. **45**, 568-572
45 McCoy, A. J., Grosse-Kunstleve, R. W., Storoni, L. C. and Read, R. J. (2005) Likelihood-enhanced fast translation functions. Acta crystallographica. Section D, Biological crystallography. **61**, 458-464
46 Emsley, P. and Cowtan, K. (2004) Coot: model-building tools for molecular graphics. Acta crystallographica. Section D, Biological crystallography. **60**, 2126-2132

47 Jesu Jaya Sudan, R. and Sudandiradoss, C. (2012) Pattern prediction and coordination geometry analysis from cadmium-binding proteins: a computational approach. Acta crystallographica. Section D, Biological crystallography. **68**, 1346-1358
48 Schuck, P. (2000) Size-distribution analysis of macromolecules by sedimentation velocity ultracentrifugation and lamm equation modeling. Biophys J. **78**, 1606-1619
49 Bertinetti, D., Schweinsberg, S., Hanke, S. E., Schwede, F., Bertinetti, O., Drewianka, S., Genieser, H. G. and Herberg, F. W. (2009) Chemical tools selectively target components of the PKA system. BMC Chem Biol. **9**, 3
50 Herberg, F. W., Maleszka, A., Eide, T., Vossebein, L. and Tasken, K. (2000) Analysis of A-kinase anchoring protein (AKAP) interaction with protein kinase A (PKA) regulatory subunits: PKA isoform specificity in AKAP binding. J Mol Biol. **298**, 329-339
51 Maass, P. G., Aydin, A., Luft, F. C., Schachterle, C., Weise, A., Stricker, S., Lindschau, C., Vaegler, M., Qadri, F., Toka, H. R., Schulz, H., Krawitz, P. M., Parkhomchuk, D., Hecht, J., Hollfinger, I., Wefeld-Neuenfeld, Y., Bartels-Klein, E., Muhl, A., Kann, M., Schuster, H., Chitayat, D., Bialer, M. G., Wienker, T. F., Ott, J., Rittscher, K., Liehr, T., Jordan, J., Plessis, G., Tank, J., Mai, K., Naraghi, R., Hodge, R., Hopp, M., Hattenbach, L. O., Busjahn, A., Rauch, A., Vandeput, F., Gong, M., Ruschendorf, F., Hubner, N., Haller, H., Mundlos, S., Bilginturan, N., Movsesian, M. A., Klussmann, E., Toka, O. and Bahring, S. (2015) PDE3A mutations cause autosomal dominant hypertension with brachydactyly. Nat Genet. **47**, 647-653
52 Stefan, E., Wiesner, B., Baillie, G. S., Mollajew, R., Henn, V., Lorenz, D., Furkert, J., Santamaria, K., Nedvetsky, P., Hundsrucker, C., Beyermann, M., Krause, E., Pohl, P., Gall, I., MacIntyre, A. N., Bachmann, S., Houslay, M. D., Rosenthal, W. and Klussmann, E. (2007) Compartmentalization of cAMP-dependent signaling by phosphodiesterase-4D is involved in the regulation of vasopressin-mediated water reabsorption in renal principal cells. J Am Soc Nephrol. **18**, 199-212
53 Sarma, G. N., Kinderman, F. S., Kim, C., von Daake, S., Chen, L., Wang, B. C. and Taylor, S. S. (2010) Structure of D-AKAP2:PKA RI complex: insights into AKAP specificity and selectivity. Structure. **18**, 155-166
54 Schrödinger Release 2015-1: Maestro, v., Schrödinger, LLC, New York, NY. (2015)
55 Horner, A., Goetz, F., Tampe, R., Klussmann, E. and Pohl, P. (2012) Mechanism for targeting the A-kinase anchoring protein AKAP18delta to the membrane. J Biol Chem. **287**, 42495-42501
56 Smith, F. D., Reichow, S. L., Esseltine, J. L., Shi, D., Langeberg, L. K., Scott, J. D. and Gonen, T. (2013) Intrinsic disorder within an AKAP-protein kinase A complex guides local substrate phosphorylation. eLife. **2**, e01319
57 Gold, M. G., Smith, F. D., Scott, J. D. and Barford, D. (2008) AKAP18 contains a phosphoesterase domain that binds AMP. J Mol Biol. **375**, 1329-1343

Figure 1

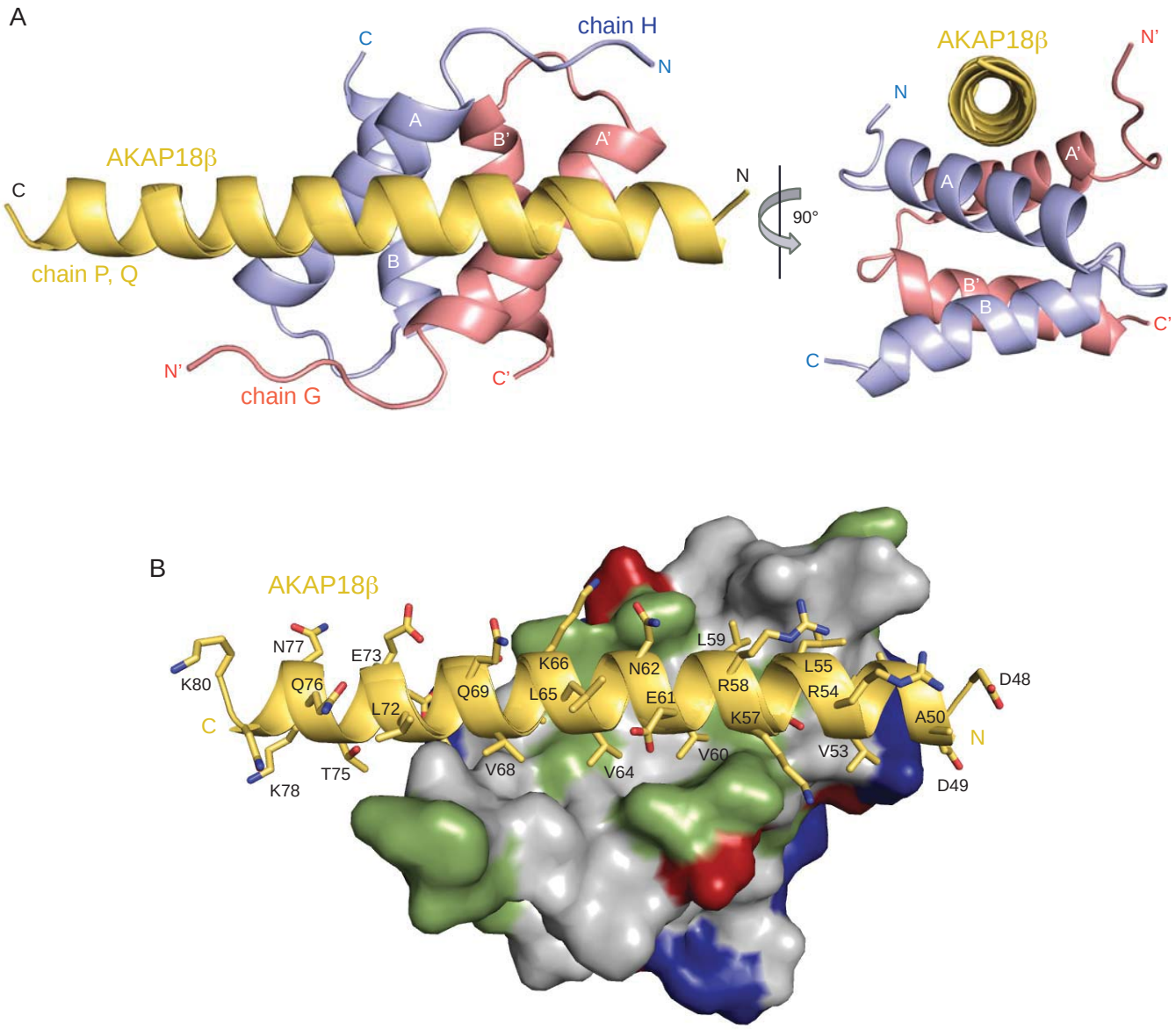
A
chain H
C
N
A
B'
A'
AKAP18β
C
N
chain P, Q
B
N'
chain G
C'
90°
AKAP18β
N'
N
A'
A
B'
B
C'
C
B
AKAP18β
N77
E73
K66
L59
K80
Q76
Q69
N62
L55
D48
L72
L65
E61
R58
R54
C
K57
A50
N
T75
V68
V64
V60
V53
K78
D49

Figure 2

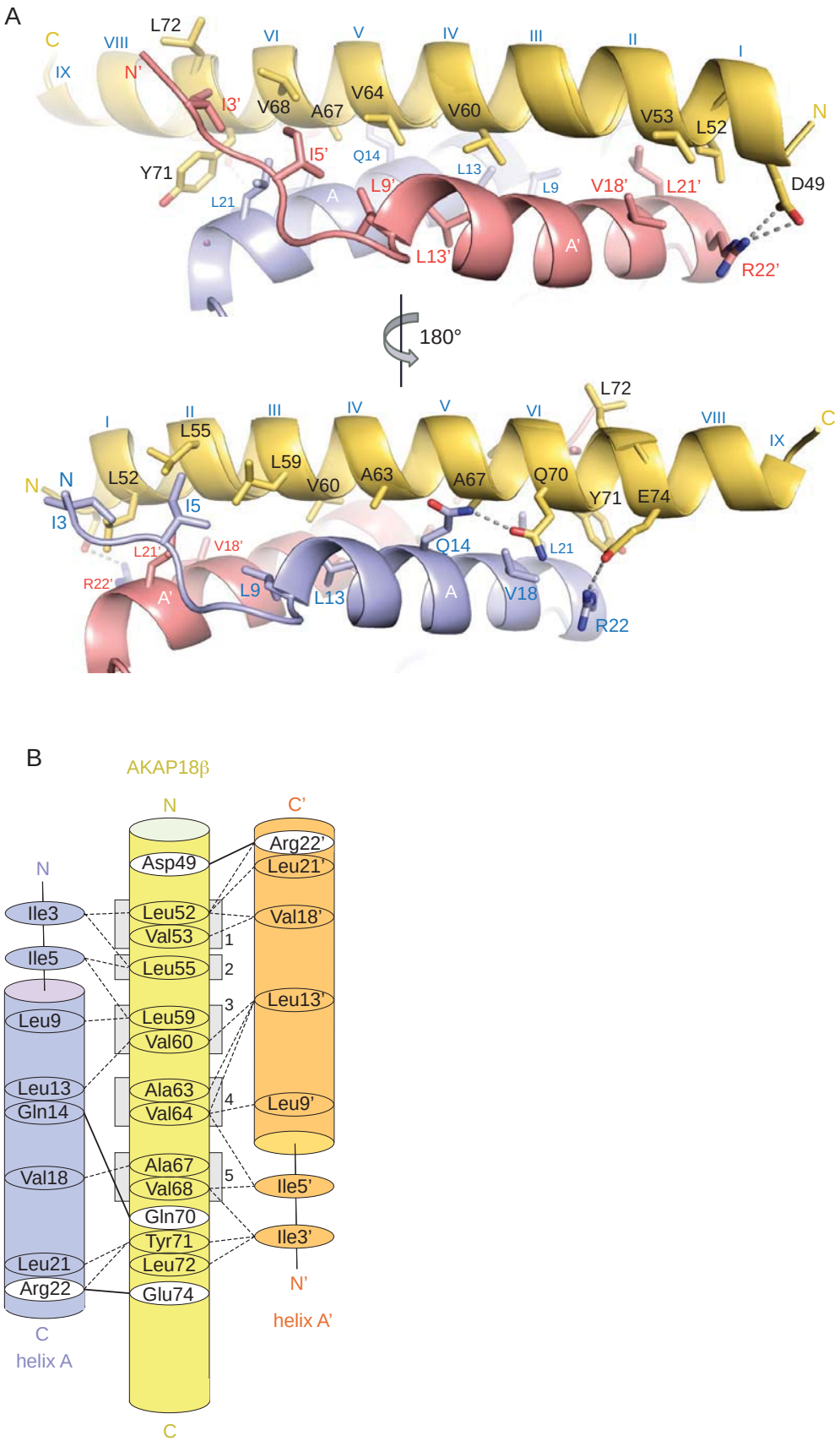
A
C
VIII
IX
N'
L72
VI
V
IV
III
II
I
N
I3'
V68
A67
V64
V60
V53
L52
I5'
Q14
L13
Y71
L9'
L9
V18'
L21'
D49
L21
A
A'
L13'
R22'
180°
L72
I
II
III
IV
V
VI
VIII
IX
C
L55
L59
N
N
L52
V60
A63
A67
Q70
Y71
E74
I5
I3
L21'
V18'
Q14
L21
R22'
A'
L9
L13
A
V18
R22
B
AKAP18β
N
C'
N
Asp49
Arg22'
Leu21'
Ile3
Leu52
Val53
Val18'
1
Ile5
Leu55
2
Leu13'
Leu9
Leu59
3
Val60
Leu13
Ala63
Leu9'
Gln14
Val64
4
Ala67
Val18
Val68
5
Ile5'
Gln70
Ile3'
Tyr71
Leu21
Leu72
N'
Arg22
Glu74
C
helix A
helix A'
C

Figure 3

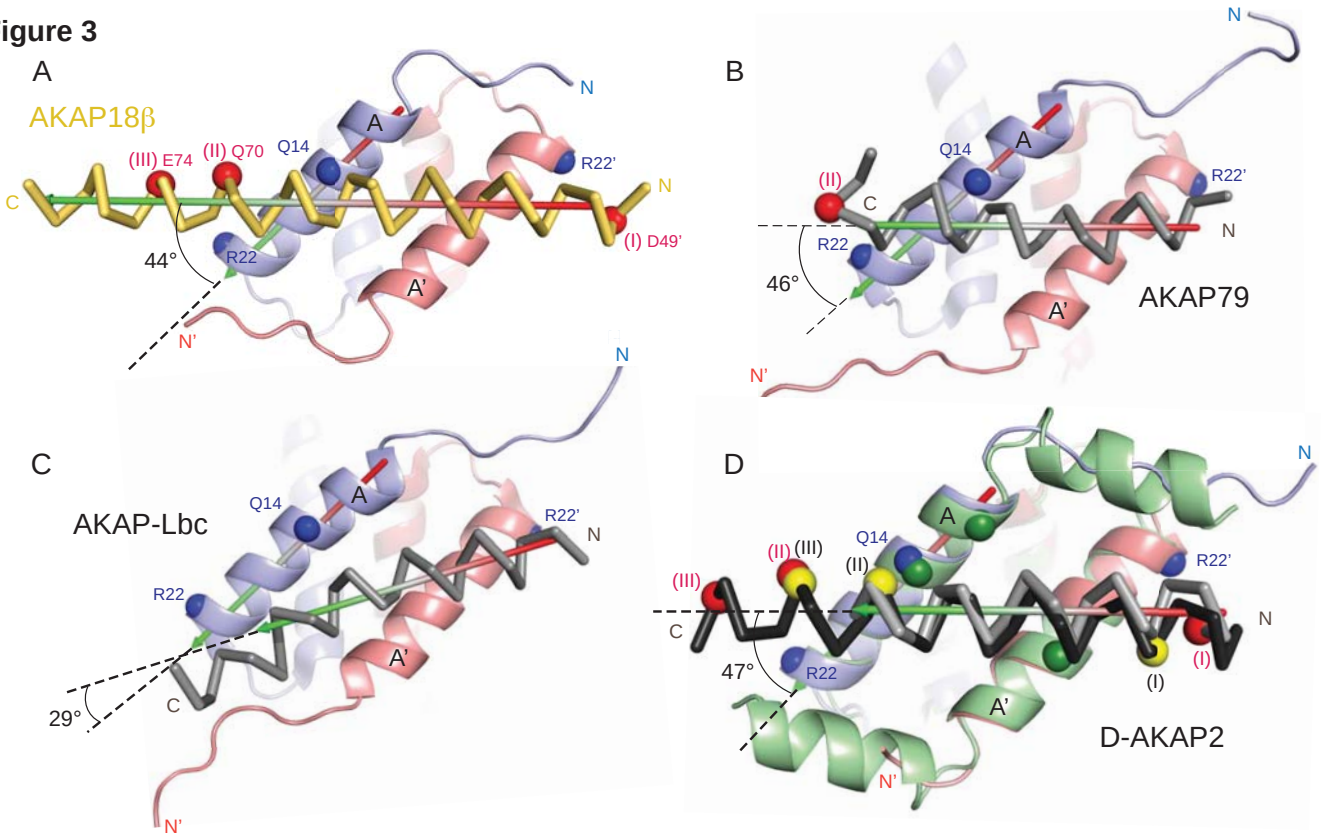

E

		I 1 2 3 5 II III	
		* ** * ** * ** *** *	
AKAP18β	(AKAP7β)	NGGEPDDAELVRLSKRLVENAVLKAVQQYLEETQNKNKPGE	
		49 70 74	
AKAP18α	(AKAP7α)	NGGEPDDAELVRLSKRLVENAVLKAVQQYLEETQNKNKPGE	
AKAP18δ	(AKAP7δ)	DRKEPEDAELVRLSKRLVENAVLKAVQQYLEETQNKKQPGE	
AKAP6	(mAKAP)	HQKDAEDCSVHNFVKEIIDMASTALKSKSQPENEVAAPTSL	
AKAP14		TQDKNYEDELTQVALALVEDVINYAVKIVEEERNPLKNIKW	
AKAP2	(AKAP-KL)	SVDDPLEYQAGLLVQNAIQQAIAEQVDKAVSKTSRDGAEQQ	RII
AKAP12	(gravin)	NGILELETKSSKLVQNIIQTAVDQFVRTEETATEMLTSELQ	
AKAP8	(AKAP95)	TPEEVAADVLAEVITAAVRAVDGEGAPAPESSGEPAEDEGP	
AKAP13	(AKAP-Lbc)	APLPKGADLIEEAASRIVDAVIEQVKAAGALLTEGEACHMS	
AKAP9	(AKAP450)	KIVNLQKIVEEKVAAALVSQIQLEAVQEYAKFCQDNQTISS	
GSKIP		TDMKDMRLEAEAVVNDVLFAVNNMFVSKSLRCADDVAYINV	
AKAP5	(AKAP79)	RTSEQYETLLIETASSLVKNAIQLSIEQLVNEMASDDNKIN	
AKAP10	(D-AKAP2)	NTDEAQEELAWKIAKMIVSDIMQQAQYDQPLEKSTKL	
Ezrin		DQIKSQEQLAAELLAEYTAKIALLEEARRRKEDEVEEWQHR	
AKAP1	(D-AKAP1)	EEGLDRNEEIKRAAFQIISQVISEATEQVLATTVGKVAGRV	
AKAP3		QLGNGSSVDEVSFYANRLTNLVIAMARKEINEKIDGSENKCV	dual aligned for RII
AKAP4	(FSC1A)	DDLSFYVNRLSSLVIQMAHKEIKEKLEGKSKCLHHSICPSP	
AKAP11	(AKAP220)	VNLDKKAVLAEKIVAEAIEKAERELSSTSLAADSGIGQEGA	
MAP2D		ADRETAEEVSARIVQVVTAEAVAVLKGEQEKEAQHKDQTAA	
		I 1 2 3 II 4 III5	
AKAP5	(AKAP79)	RTSEQYETLLIETASSLVKNAIQLSIEQLVNEMASDDNKIN	
AKAP10	(D-AKAP2)	NTDEAQEELAWKIAKMIVSDIMQQAQYDQPLEKSTKL	
Ezrin		DQIKSQEQLAAELLAEYTAKIALLEEARRRKEDEVEEWQHR	
AKAP1	(D-AKAP1)	EEGLDRNEEIKRAAFQIISQVISEATEQVLATTVGKVAGRV	
AKAP3		QLGNGSSVDEVSFYANRLTNLVIAMARKEINEKIDGSENKC	dual aligned for RI
AKAP4	(FSC1A)	DDLSFYVNRLSSLVIQMAHKEIKEKLEGKSKCLHHSICPSP	
AKAP11	(AKAP220)	VNLDKKAVLAEKIVAEAIEKAERELSSTSLAADSGIGQEGA	
MAP2D		ADRETAEEVSARIVQVVTAEAVAVLKGEQEKEAQHKDQTAA	
AKAP$_{CE}$		IEESANESALYQFADRFSELVISEALNHRKMHYDPAVKEFY	
AKAP4	(FSC1B)	EFADSISKGLMVYANQVASDMMVSLMKTLKVHSSGKPIPAS	
smAKAP		GTNTVILEYAHRLSQDILCDALQQWACNNIKYHDIPYIESE	RI
SKIP		PDIYCITDFAEELADTVVSMATEEIAAICLDNSSGKQPWFC	
PAP7		RLEQQKQQIMAALNSQTAVQFQQYAAQRYPGNYEQQQILIR	

Figure 4

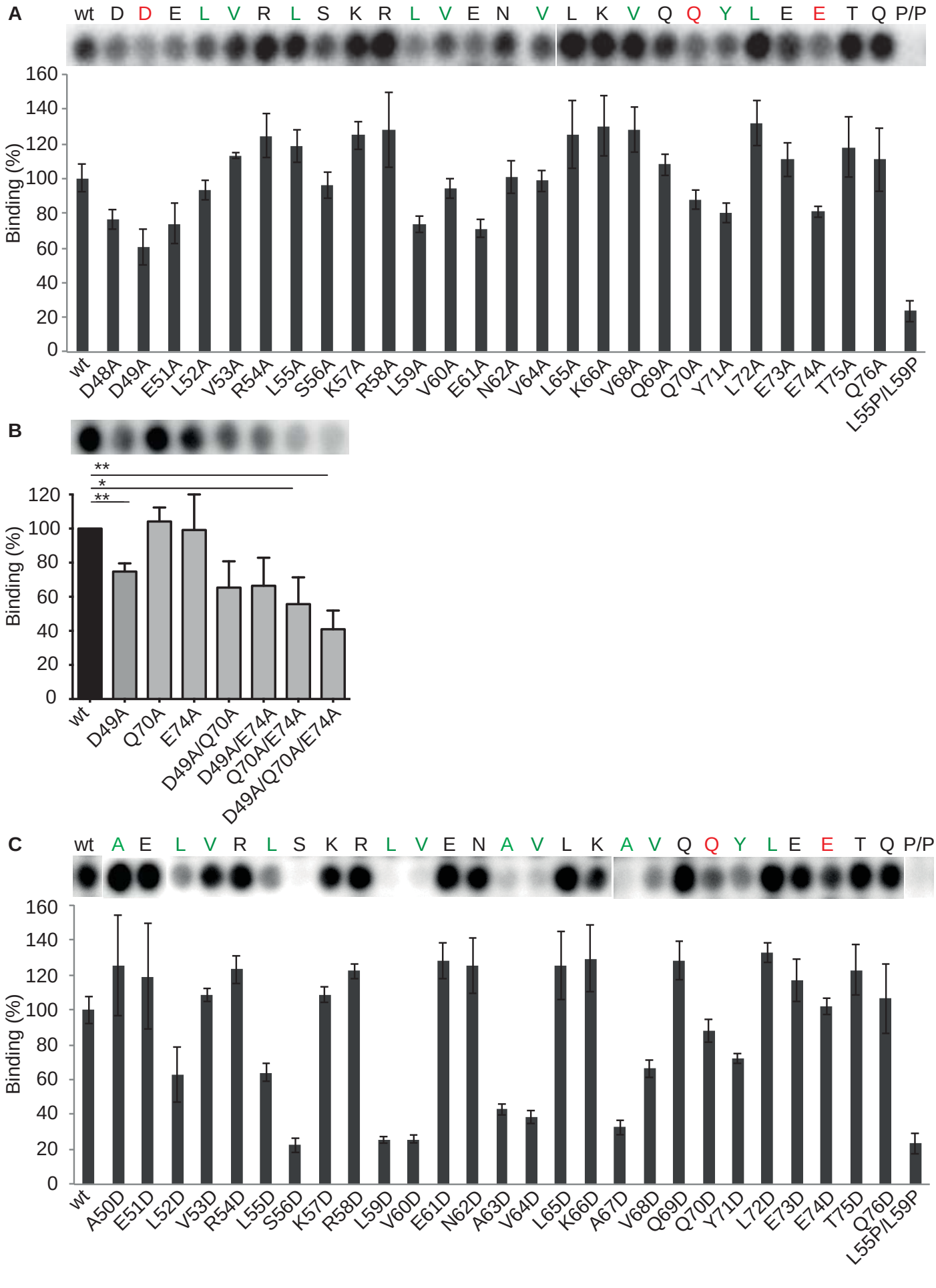
A
wt D D E L V R L S K R L V E N V L K V Q Q Y L E E T Q P/P
Binding (%)
0 20 40 60 80 100 120 140 160
wt D48A D49A E51A L52A V53A R54A L55A S56A K57A R58A L59A V60A E61A N62A V64A L65A K66A V68A Q69A Q70A Y71A L72A E73A E74A T75A Q76A L55P/L59P
B
**
*
**
Binding (%)
0 20 40 60 80 100 120
wt D49A Q70A E74A D49A/Q70A D49A/E74A Q70A/E74A D49A/Q70A/E74A
C
wt A E L V R L S K R L V E N A V L K A V Q Q Y L E E T Q P/P
Binding (%)
0 20 40 60 80 100 120 140 160
wt A50D E51D L52D V53D R54D L55D S56D K57D R58D L59D V60D E61D N62D A63D V64D L65D K66D A67D V68D Q69D Q70D Y71D L72D E73D E74D T75D Q76D L55P/L59P

Figure 5

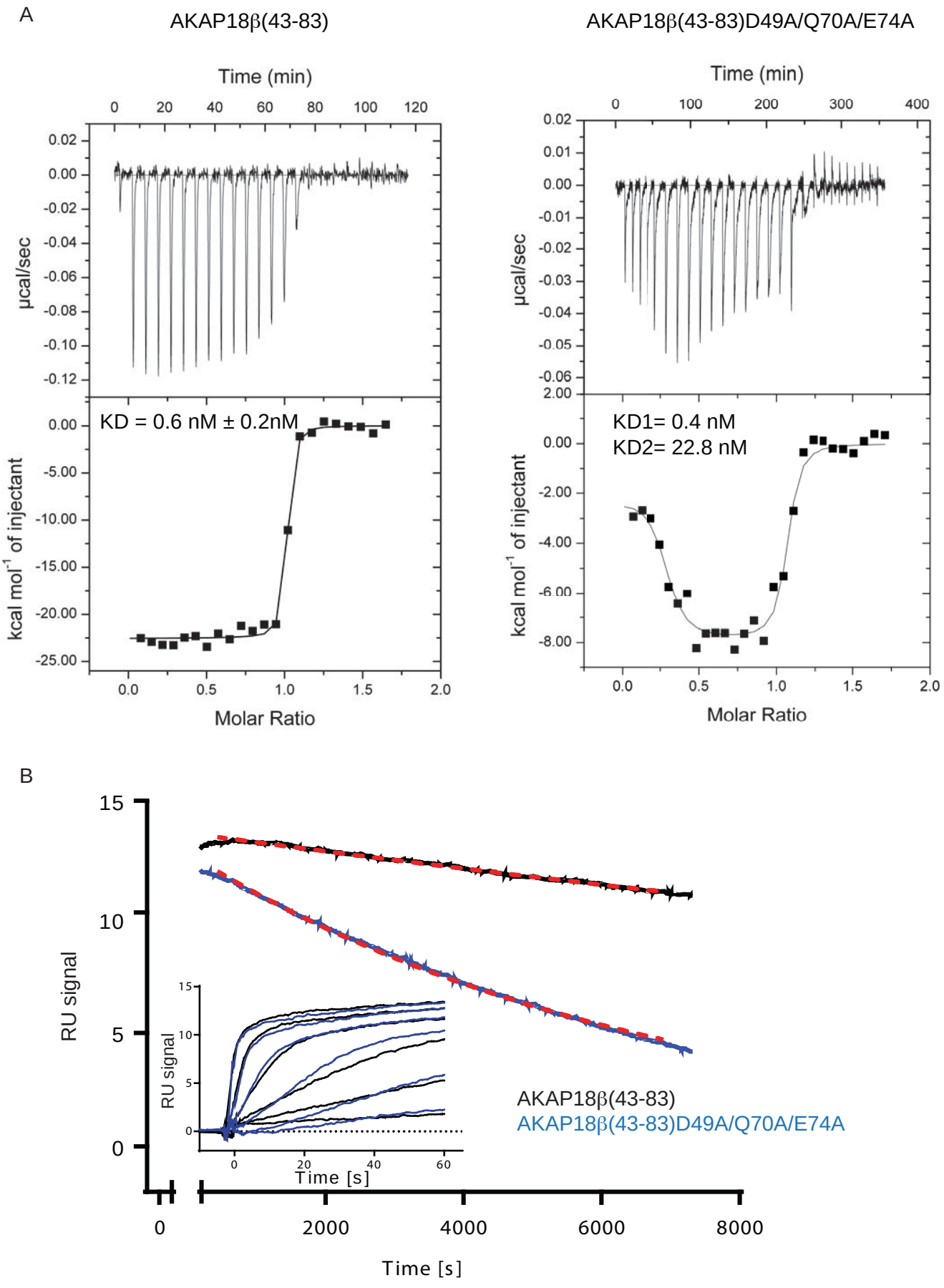
A
AKAP18β(43-83)
AKAP18β(43-83)D49A/Q70A/E74A
Time (min)
µcal/sec
kcal mol-1 of injectant
KD = 0.6 nM ± 0.2nM
KD1= 0.4 nM
KD2= 22.8 nM
Molar Ratio
B
RU signal
Time [s]
AKAP18β(43-83)
AKAP18β(43-83)D49A/Q70A/E74A

Figure 6

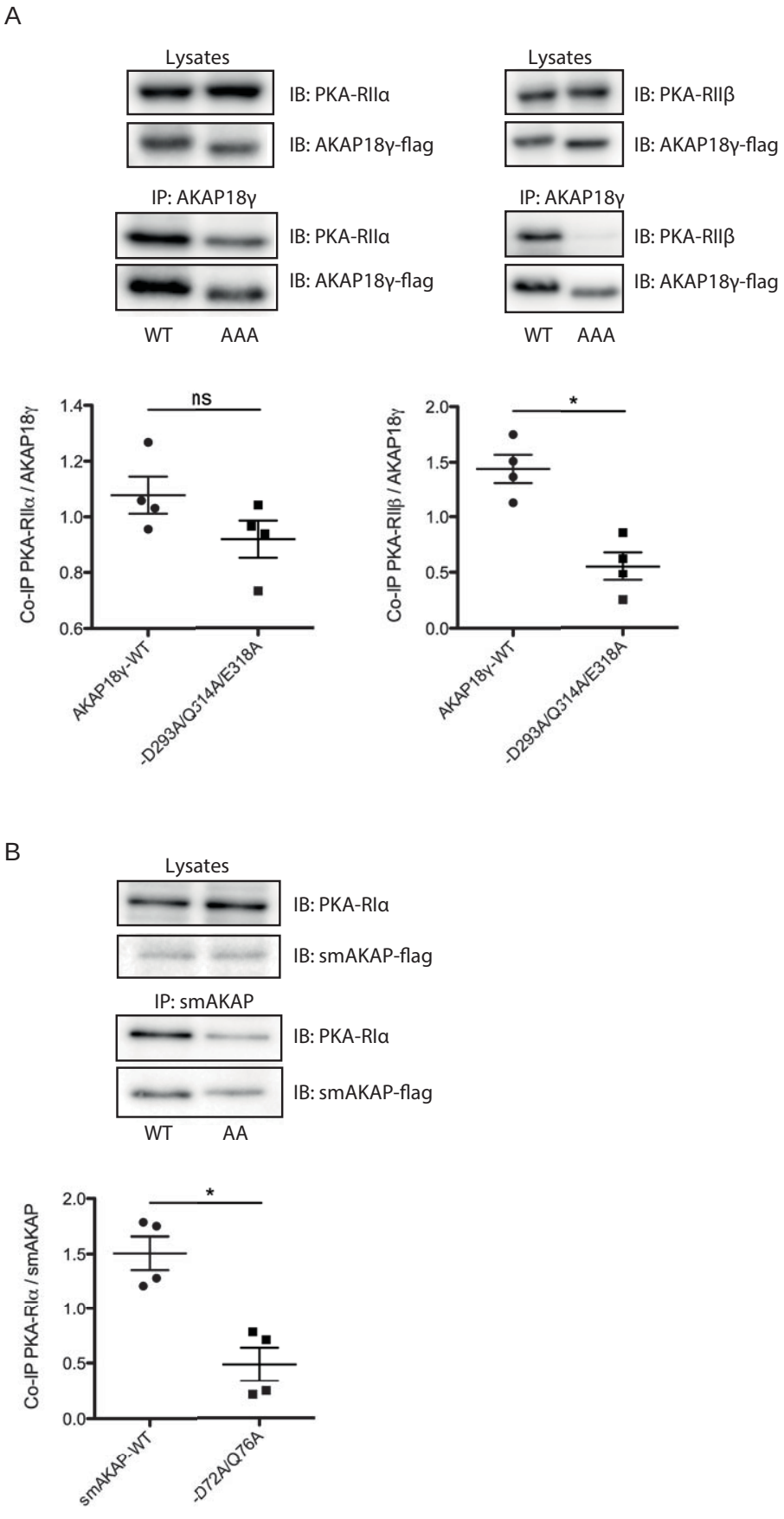
A
Lysates
IB: PKA-RIIα
IB: AKAP18γ-flag
IP: AKAP18γ
IB: PKA-RIIα
IB: AKAP18γ-flag
WT
AAA
Lysates
IB: PKA-RIIβ
IB: AKAP18γ-flag
IP: AKAP18γ
IB: PKA-RIIβ
IB: AKAP18γ-flag
WT
AAA
Co-IP PKA-RIIα / AKAP18γ
ns
1.4
1.2
1.0
0.8
0.6
AKAP18γ-WT
-D293A/Q314A/E318A
Co-IP PKA-RIIβ / AKAP18γ
*
2.0
1.5
1.0
0.5
0.0
AKAP18γ-WT
-D293A/Q314A/E318A
B
Lysates
IB: PKA-RIα
IB: smAKAP-flag
IP: smAKAP
IB: PKA-RIα
IB: smAKAP-flag
WT
AA
Co-IP PKA-RIα / smAKAP
*
2.0
1.5
1.0
0.5
0.0
smAKAP-WT
-D72A/Q76A